



# Reconstructing hydrophobic ZIF-8 crystal into hydrophilic hierarchically-porous nanoflowers as catalyst carrier for nonenzymatic glucose sensing

Qizhen Zhu<sup>a</sup>, Shiyu Hu<sup>a</sup>, Linqun Zhang<sup>b</sup>, Ying Li<sup>a,c,d,\*</sup>, Carlo Carraro<sup>c,d</sup>, Roya Maboudian<sup>c,d</sup>, Wei Wei<sup>a</sup>, Anran Liu<sup>a</sup>, Yuanjian Zhang<sup>a</sup>, Songqin Liu<sup>a</sup>

<sup>a</sup> Jiangsu Engineering Laboratory of Smart Carbon-Rich Materials and Device, School of Chemistry and Chemical Engineering, Southeast University, Nanjing 211189, China

<sup>b</sup> Analytical & Testing Center, Nanjing Normal University, Nanjing 210023, China

<sup>c</sup> Berkeley Sensor & Actuator Center, University of California, Berkeley, California 94720, USA

<sup>d</sup> Department of Chemical and Biomolecular Engineering, University of California, Berkeley, California 94720, USA

## ARTICLE INFO

### Keywords:

Hydrophilicity

Hierarchically-pore

ZIF-8

Cu nanoparticle

Non-enzymatic glucose sensor

Organic weak acid

## ABSTRACT

ZIF-8, a zeolite-type metal-organic framework (MOF), is an effective carrier to support nanocatalysts for applications in the catalysis areas due to its high chemical and thermal stability, and unique structure. The ability to reconstruct the structure of ZIF-8 opens up the potential to enhance its performance in catalysis. In this work, the structure of hydrophobic ZIF-8 crystal is engineered to form hydrophilic hierarchically-porous nanoflowers (HHNs) by using an organic weak acid as etchant. Results reveal that besides imparting hydrophilicity to ZIF-8, the uniform micropores in ZIFs are transformed to mesopores and macropores, which are beneficial to nanoparticle immobilization and electrochemical reactions. After incorporating Cu nanoparticles into the matrix HHNs, the composite Cu@HHNs manifest superior catalytic activities for glucose electro-catalytic oxidation under alkaline media, compared with Cu nanoparticles loaded on untreated ZIF-8. The proposed Cu@HHNs based sensor displays exceptional sensing performances with a linear range of 5  $\mu\text{M}$  to 3 mM, a detection limit of 1.97  $\mu\text{M}$  (signal-to-noise ratio (S/N) of 3), a sensitivity of 1594.2  $\mu\text{A mM}^{-1} \text{cm}^{-2}$ , and high selectivity, specificity, and reproducibility. In addition, Cu@HHNs can be utilized for glucose sensing in human blood serum, demonstrating its feasibility toward determination of glucose for practical sample testing.

## 1. Introduction

Glucose is an indispensable nutrient directly involved in the metabolic activities in the human microenvironment. However, an excess of glucose in human blood is damaging to human health, which could result in diabetes mellitus and other complications [1]. The diabetes mellitus could endanger one's physical condition to disability and even death if it is not controlled [2]. Therefore, it is of great significance to detect the concentration level of glucose in blood precisely in order to implement the diagnosis, treatment and management of diabetes mellitus [3–5].

The glucose electrochemical biosensors have undergone long-term development from enzymatic sensors to non-enzymatic sensors [6,7]. It is well-known that enzymes are intrinsically unstable and inevitably expensive despite their high sensitivity and selectivity. Furthermore, the applications of enzymes are confined by many other factors such as pH, temperature, humidity and the dependence on oxygen [8,9].

Therefore, many current research activities are focusing on non-enzymatic electrochemical glucose biosensors [10]. Over the past decades, Cu-based nanomaterials, such as various Cu nanoparticles, alloys, oxides and hydroxides, have drawn extensive attention owing to the natural abundance of copper, and its low cost and excellent electrocatalytic properties [8,11–13]. To mention a few, Li et al. successfully utilized polymeric micelles as soft templates to fabricate a connected mesoporous Cu film, which exhibited good performance toward glucose electro-oxidation with a sensitivity of 606  $\mu\text{A mM}^{-1} \text{cm}^{-2}$  [14]. Li et al. fabricated bimetallic Cu-Ag nanocomposites with a rough surface and porous flexural algae-like microstructure for non-enzymatic glucose detection [15]. The as-prepared Cu-Ag sensor showed enhanced electrocatalytic activity, significant selectivity, excellent stability, good reproducibility, and attractive feasibility for real sample analysis. Gao et al. synthesized mesocrystalline  $\text{Cu}_2\text{O}$  hollow nanocubes with oriented aggregation structure, which exhibit high electro-catalytic activity for glucose oxidation [16].

\* Corresponding author at: Jiangsu Engineering Laboratory of Smart Carbon-Rich Materials and Device, School of Chemistry and Chemical Engineering, Southeast University, Nanjing 211189, China.

E-mail address: [yingli@seu.edu.cn](mailto:yingli@seu.edu.cn) (Y. Li).

<https://doi.org/10.1016/j.snb.2020.128031>

Received 28 January 2020; Received in revised form 2 March 2020; Accepted 21 March 2020

Available online 04 April 2020

0925-4005/© 2020 Elsevier B.V. All rights reserved.



However, nanoparticles are prone to migration and aggregation during synthesis and reaction processes due to their high surface energy, resulting in the deactivation of nanoparticle catalysts. To address this problem, using porous materials as catalyst supports for nanoparticle catalysts is regarded as one of the most effective ways [17–20]. As a subfamily of metal organic frameworks (MOFs), zeolitic imidazolate frameworks (ZIFs) have become particularly promising framework supports for Cu nanoparticle immobilization due to their sturdy porosity, and excellent thermal and chemical stability [21,22]. ZIFs possess zeolitic structural features, in which Zn metal ions are tetrahedrally coordinated with the N atoms of the organic imidazole ligands and the angles between metal-imidazole-metal units are similar to those of Si-O-Si in zeolites [21]. The nitrogen atoms in ZIF-8 effectively limit the migration and aggregation of small active catalytic nanoparticles (NPs) in the solid state, consequently making the NPs-on-MOF catalysts highly active and reusable. Shi et al. incorporated Cu NPs into ZIF-8 for fabrication of non-enzymatic glucose sensor, which exhibited a higher electro-catalytic performance than simply loading Cu NPs on ZIF-8 with the sensitivity of  $418 \mu\text{A mM}^{-1} \text{cm}^{-2}$  and an impressive stability owing to its unique ZIF-8-encapsulated structure [22]. However, the diameters of the intrinsic open channels in ZIF-8 are smaller than 2 nm. Such small pores can hinder the incorporation of large-sized guest nanoparticles and restrict the diffusion efficiency of reactants and products inside the bulk of ZIF-8 [23,24]. Moreover, the poor electronic conductivity and low wettability of ZIF-8 not only are unfavorable for the transport and collection of the electrons, but also block the contact and mass transfer between the electrode material and the electrolyte during the electro-catalytic processes. These drawbacks hinder the ZIF-8 matrix from being an ideal carrier to load electro-catalyst. Since the structure of catalyst matrix is a crucial factor for the catalysis performance, engineering the structure and surface of ZIF-8 will afford it desirable properties in catalysis.

In this paper, we demonstrate the reconstruction of hydrophobic ZIF-8 crystal to form composite nanoflowers with hydrophilic surface and hierarchy-porous structure through the treatment with gallic acid (GA), as shown in Scheme 1. As a weak organic phenolic acid, gallic acid can release free protons to be combined with the N atoms of imidazole, which are initially bonded to metal nodes in ZIF-8, damaging the ZIF-8 framework. Meanwhile, GA has the conjugate rigid plane, high absorbability of O atoms and larger molecular size than imidazole, which can prevent the ZIF-8 matrix from fully collapsing. Therefore, the acid etching procedure can reconstruct the crystalline ZIF-8 bulk into three-dimensional hierarchically-porous structure consisting of two-dimensional sheet-like structure, and exposing the N atoms and Zn ions, which were otherwise buried deeply in the ZIF-8 matrix. Both N atoms and Zn ions have strong polarity. On one hand, the strong polarity helps with the immobilization of guest nanoparticles

and enhances their dispersibility and stability. On the other hand, it can improve the hydrophilic property of the material, which is favorable for the occurrence of electro-catalytic reaction in the water phase (such as glucose electrochemical oxidation). In addition, the pores of the material have been widened up from micro-pores to meso-pores and even macro-pores, which are beneficial for the efficient diffusion of the reactants and products during the electro-catalytic process [25]. Subsequently, Cu NPs as a model were loaded on the as-synthesized HHNs (Scheme 1) to prepare the catalyst Cu@HHNs for glucose electrochemical detection. For comparison, the electrochemical performance of Cu NPs loaded on ZIF-8 (Cu@ZIF-8) was also investigated. It is found that Cu@HHNs exhibited enhanced activity, favorable sensitivity, satisfactory selectivity, and excellent stability for long life test toward the oxidation of glucose in alkaline media. In addition, Cu@HHNs was utilized for glucose sensing in human blood serum, demonstrating its feasibility toward glucose determination for practical sample testing. The results prove that the acid-treated HHNs can serve as an excellent substrate to load metal nanoparticles for constructing various biosensors.

## 2. Experimental

Materials, apparatus and electrochemical measurements are presented in supplementary materials.

### 2.1. Synthesis of ZIF-8

ZIF-8 was synthesized following previously published processes [26]. In brief, 1.485 g  $\text{Zn}(\text{NO}_3)_2 \cdot 6\text{H}_2\text{O}$  and 3.280 g 2-methylimidazole were separately dispersed in 50 mL methanol, and then, the two solutions were mixed. After vigorous agitation for 2 h at room temperature, a white suspension was obtained. A ZIF-8 nanopolyhedra (white powder) was acquired after centrifugation, wash with methanol and freeze-drying.

### 2.2. Etching of ZIF-8

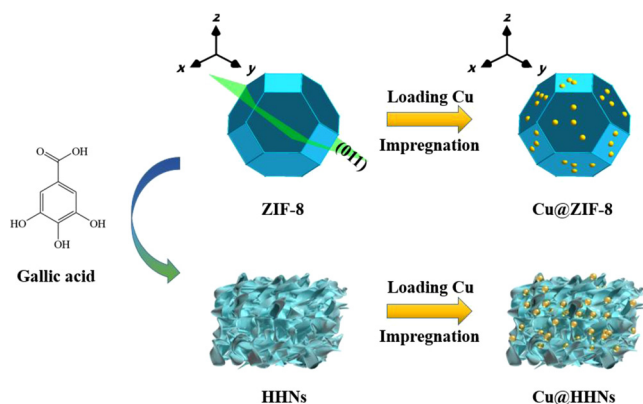
Typically, 300 mg ZIF-8 powder was dispersed in 75 mL ultrapure water. Then, 750 mg GA in 75 mL ultrapure water was quickly added into the ZIF-8 suspension. After vigorous agitation for 5 min at room temperature, during which the etching process was in progress, a white suspension was obtained. Hereafter, the white suspension was suction-filtered and rinsed with ultrapure water. At last, the resulting product was freeze-dried overnight, yielding the hydrophilic hierarchically-porous nanoflowers, HHNs.

### 2.3. Synthesis of Cu@ZIF-8 and Cu@HHNs

Cu@HHNs were synthesized via an impregnation method, along with subsequent reduction of the precursor. In detail, 100.0 mg HHNs powder and 105.2 mg  $\text{CuCl}_2 \cdot 2\text{H}_2\text{O}$  were respectively dispersed in 20 mL ultrapure water. After continuously stirring the mixture for 6 h in order to allow sufficient blending, the impregnation procedure was accomplished and  $\text{Cu}^{2+}$  ions were incorporated in the inner pores and channels of HHNs. Hereafter, 3.1 mL freshly prepared aqueous solution of  $\text{NaBH}_4$  (1 M) was added into the bluish  $\text{Cu}^{2+}$ /HHNs and the color of the mixture turned black instantly. To ensure the thorough reduction of  $\text{Cu}^{2+}$ , the mixture was stirred for 2 h at room temperature. Eventually, the resulting product was suction-filtered, washed with water for three times, freeze-dried overnight and the desired catalyst Cu@HHNs was acquired. For comparison, Cu@ZIF-8 was also synthesized according to the same controlled procedure.

### 2.4. Fabrication of the Cu@HHNs based sensors

In this work, a commercial glassy carbon electrode (GCE) was used,



**Scheme 1.** The scheme of reconstruction of hydrophobic ZIF-8 crystal into hydrophilic hierarchy-porous nanoflowers via organic weak acid etching as a carrier for Cu nanoparticles.



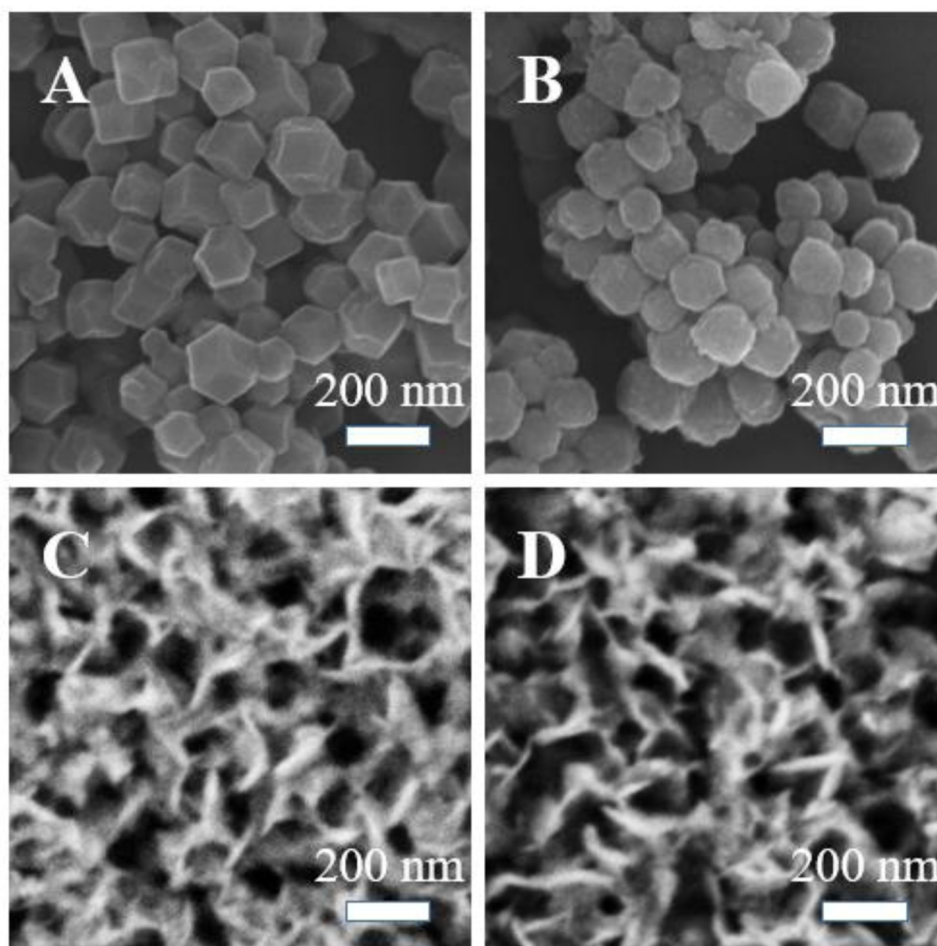


Fig. 1. FE-SEM images of (A) ZIF-8, (B) Cu@ZIF-8, (C) HHNs, and (D) Cu@HHNs.

with the effective working area of  $0.071 \text{ cm}^2$ . 2 mg catalyst was dispersed into 1 mL ultrapure water to form a uniform suspension. After sonication for adequate time, 8  $\mu\text{L}$  of the as-prepared catalyst dispersion was drop-casted onto the prepared GCE. The loading of the catalyst on GCE is calculated to be  $0.22 \text{ mg/cm}^2$ . After the catalyst was dried, 5  $\mu\text{L}$  of Nafion solution (0.05 wt%) was drop-casted over the GCE. Since there is only physical absorption between the catalyst and the electrode, Nafion solution was used as a binder to protect active materials from dropping or dissolving in the electrolyte. These as-prepared electrodes were desiccated and stored in  $40^\circ\text{C}$  oven for further use.

### 3. Results and discussions

#### 3.1. Materials characterizations

Field-emission scanning electron microscope (FE-SEM) was implemented to observe the surface morphology of the materials at various stages (Scheme 1). As shown in Fig. 1, ZIF-8 possesses good crystal morphology, consisting of uniform rhombic dodecahedron structure, with a particle size distribution mostly concentrated around 200 nm. After the incorporation of Cu NPs into ZIF-8, although the crystalline size of the ZIF-8 matrix is retained, the morphology has changed slightly, suggesting that the ZIF matrix maintains its crystalline structure and most of Cu particles are loaded on the surface of the matrix. After the etching procedure, the HHN matrix is in the shape of three-dimensional hierarchically-porous structure, consisting of two-dimensional sheet-like structure. Moreover, there is no perceptible change in the morphology of the HHNs after the incorporation of the metallic copper into the matrix, suggesting that the structure of the matrix is

retained and the vast majority of Cu NPs are in the inner pores and channels instead of on the surface of HHNs. Fig. S1 displays the SEM elemental mapping of the as-synthesized Cu@HHNs. It further confirms that the elements C, N, O, Cu, and Zn have dispersed uniformly throughout the entire architecture of the proposed catalyst Cu@HHNs.

X-ray diffraction (XRD) was used to determine the crystallinity of the as-prepared material. As shown in Figs. 2 and S2, the diffraction peaks of ZIF-8 demonstrate its good crystallinity, with the spectrum in good agreement with the literature [26]. After the incorporation of Cu NPs into the matrix, the diffraction peaks of ZIF-8 show no obvious difference to those of original ZIF-8, revealing that the crystalline structure and the morphology of ZIF-8 are retained on the whole after the Cu NP incorporation. The characteristic peaks of  $\text{CuO} \cdot 3\text{H}_2\text{O}$  (for instance, (110) crystalline plane at  $2\theta = 20.8^\circ$ ), characteristic peaks of  $\text{Cu}(\text{OH})_2$  (for instance, (111) crystalline plane at  $2\theta = 36.5^\circ$ ) and characteristic peaks of Cu (for instance, (111) crystalline plane at  $2\theta = 43^\circ$ ) show the existence of Cu, CuO and  $\text{Cu}(\text{OH})_2$  NPs in Cu@ZIF-8 [27]. After the acid etching procedure, the XRD patterns of HHNs are significantly different from those of the original ZIF-8. Although the sharp diffraction peaks of HHNs confirm their crystallinity, the broadened peak beginning at  $2\theta = 27.5^\circ$  indicates partial amorphization of HHNs caused by etching. After acid treatment, the (011) and (022) peaks of ZIF-8 are missing, confirming that the bulk crystal structure of ZIF-8 is preferentially decomposed along (011) direction. The original ZIF-8 has sharp edges and corners (Fig. 1A), which are more active than flat planes. Thus in acid solution, the edges and corners of ZIF-8 are first dissolved due to the protonation of N atoms, meanwhile the planar surfaces remain. Then, the decomposition proceeds preferably along (011) plane (Scheme 1), and nanosheets are formed. In this way, the



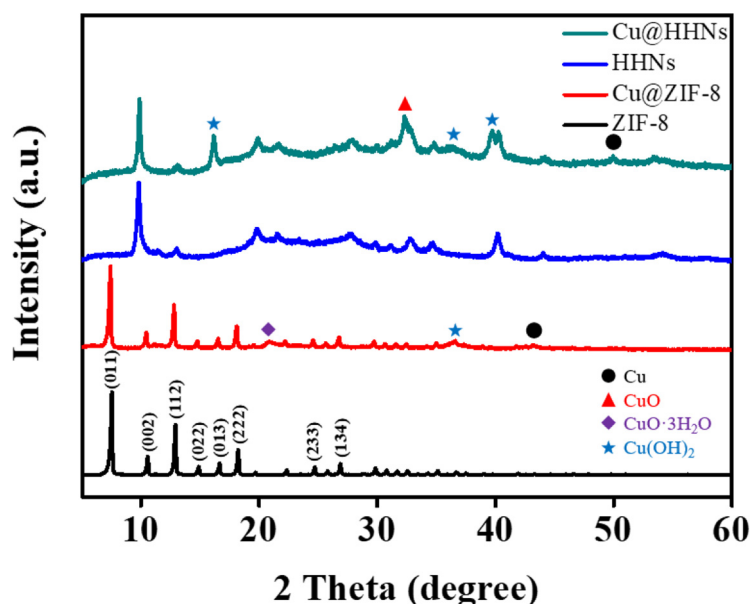


Fig. 2. XRD patterns of ZIF-8, Cu@ZIF-8, HHNs, and Cu@HHNs.

architecture of ZIF-8 is reconstructed into nanoflower structure. This etching procedure exposes the strong polar centers such as N and Zn atoms, which are buried deep inside ZIF-8 initially, being beneficial for anchoring Cu NPs. After Cu NPs are incorporated into HHNs, the material exhibits quite different XRD patterns from those loaded on ZIF-8, indicating the different crystalline structures of Cu NPs derived from the different loading matrix.

The composition and chemical state of various elements in the as-prepared materials were investigated via X-ray photoelectron spectroscopy (XPS). The survey scans (Fig. S3A) show the presence of all elements (C, N, O, Cu, and Zn) with the atomic percentages provided in Table S1. The Zn 2p region (Fig. S3B) of the catalyst Cu@HHNs involves two peaks at 1021.9 and 1045.0 eV, which are assigned to Zn 2p<sup>3/2</sup> and Zn 2p<sup>1/2</sup>, respectively [26]. This indicates that Zn<sup>2+</sup> ions still remain in this material after etching with GA, which inherit from the original matrix ZIF-8. From Fig. 3, we can see that the Cu 2p<sup>3/2</sup> regions of Cu@ZIF-8 and Cu@HHN samples are slightly different from each

other, which can be deconvoluted into two peaks at 934.76 and 932.74 eV. The higher binding energy (BE) peak at 934.76 eV is assigned to Cu<sup>2+</sup>, accompanied by the characteristic Cu<sup>2+</sup> satellite peaks ranging from 938 to 945 eV. The lower BE peak at 932.85 eV indicates the existence of Cu<sup>+</sup> or Cu<sup>0</sup> species [28,29] as the spectra cannot distinguish between the Cu<sup>+</sup> and Cu<sup>0</sup> species. The Cu LMM Auger electron spectrum confirms that besides Cu<sup>0</sup>, Cu<sup>+</sup> also exists in Cu@HHNs deduced from the peak centered at 911.40 eV [29], as shown in Fig. 3D. On the other hand, there is no Cu<sup>+</sup> in Cu@ZIF-8, as shown in Fig. 3C. Therefore, in light of the XPS results, the acid-treatment amends the chemical microenvironment of the ZIF-8, and results in the Cu NPs loaded on HHNs possessing a mixed valence state of the metallic Cu and thus constituting multiple oxidation states system. This may be expected to facilitate the redox reaction on the surface of the electrode and enhance the electro-catalytic activity of the electrode material toward non-enzymatic glucose sensing [30].

Fourier transform infrared spectra (FTIR) are presented in Fig. S4 to

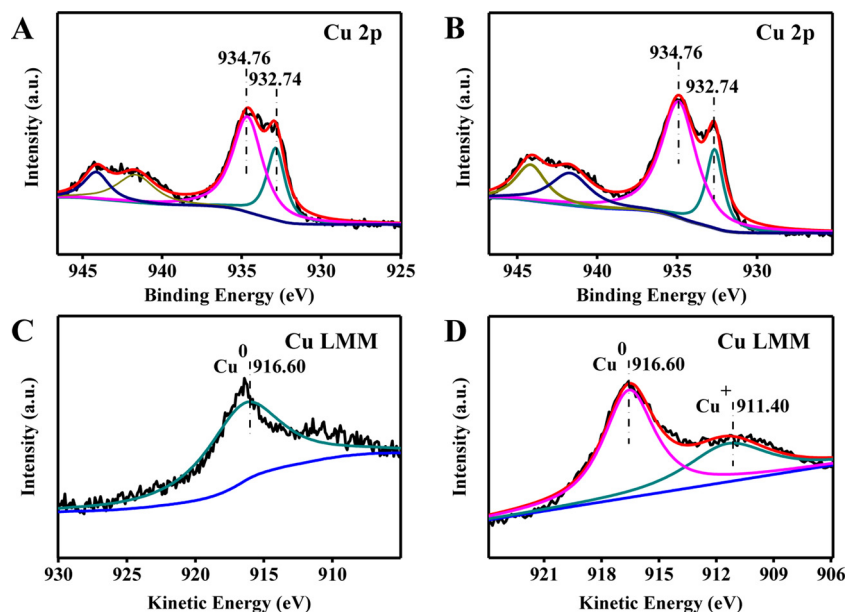


Fig. 3. Cu 2p XPS of (A) Cu@ZIF-8 and (B) Cu@HHNs; Cu LMM Auger electron spectra of (C) Cu@ZIF-8 and (D) Cu@HHNs.



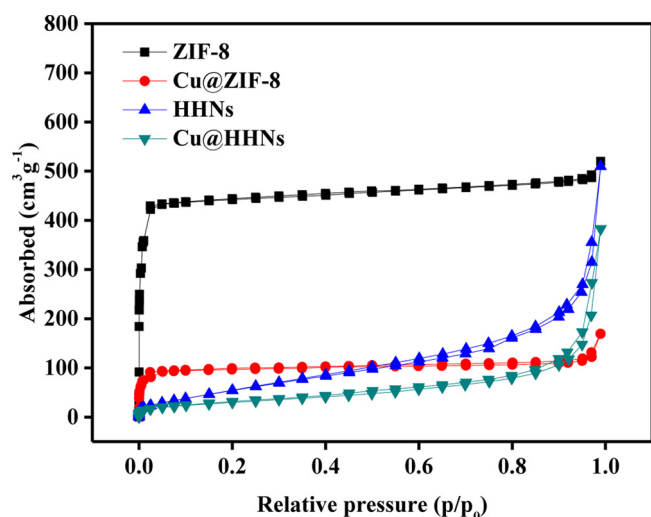


Fig. 4. Nitrogen adsorption – desorption isotherms at 77 K of (A) ZIF-8, (B) Cu@ZIF-8, (C) HHNs, and (D) Cu@HHNs.

verify the organic functional group and the chemical structure of the materials. In the HHN sample, the peak at  $3135\text{ cm}^{-1}$  represents the stretching vibration of the C–H bond in the imidazole ring, and the peak at  $2930\text{ cm}^{-1}$  represents the stretching vibration of the C–H bond in the methyl group. Both of these peaks originated from the material before etching, ZIF-8. On the other hand, the peak at  $1395\text{ cm}^{-1}$  represents the bending vibration of the –OH group, and the distinct broad peak ranging from  $3300\text{ cm}^{-1}$  to  $2500\text{ cm}^{-1}$  represents the –OH in carboxyl groups, which both originate from the gallic acid. Thus, it can be deduced that after etching, GA as a residue provides plentiful oxygen-containing functional groups that can be attached to HHN surface. The –OH in carboxyl group is different from the one in alcohol species, in that the bond between H and O atoms is prone to association. This results in carboxyl group with negative charge, which interacts with the empty orbitals of Cu. Therefore, there are more Cu–O bonds in Cu@HHNs than those in Cu@ZIF-8. That is, more massive  $\text{Cu}(\text{OH})_2$  and  $\text{CuO}\cdot\text{H}_2\text{O}$  are formed when Cu is incorporated in HHNs in comparison to Cu@ZIF-8, which is consistent with the XRD results (Fig. 2).

As depicted in Fig. 4,  $\text{N}_2$  adsorption-desorption isotherms were performed to investigate the pore structure of the materials, from which information such as specific surface area (SSA), pore volume, and pore size distribution can be acquired. The Brunauer-Emmett-Teller specific surface areas (SSA) of the ZIF-8, Cu@ZIF-8, HHNs, and Cu@HHNs are calculated to be  $1352.648\text{ m}^2\text{ g}^{-1}$ ,  $287.742\text{ m}^2\text{ g}^{-1}$ ,  $158.924\text{ m}^2\text{ g}^{-1}$ ,  $131.169\text{ m}^2\text{ g}^{-1}$ , respectively (Table S2). In addition, as illustrated in Fig. S5, the corresponding Barrett-Joyner-Halenda pore size distribution curves demonstrate that both the HHN matrix and the catalyst Cu@HHNs possess all three types of pores: micropores ( $< 2\text{ nm}$ ), mesopores ( $2\text{--}50\text{ nm}$ ) and macropores ( $> 50\text{ nm}$ ). The hierarchical micro-

meso-macro-porous structure of HHNs is propitious for incorporating the catalyst nanoparticles, while the hierarchical structure of Cu@HHNs is beneficial for efficaciously exposing the active sites of the catalytic nanoparticles and enabling efficient mass transport of molecules and ions between the electrolyte and the electrode, thereby accelerating the catalytic processes [31].

For probing the surface wettability of the as-synthesized materials, static contact angle test was carried out, as shown in Fig. S6. The surface of ZIF-8 is naturally hydrophobic with a contact angle of  $79.6 \pm 1.2^\circ$ . Hydrophobic materials block metal nanoparticle deposition inside their pores or channels due to trapped air bubbles when filled with aqueous solution, and thus Cu nanoparticles are prone to aggregate on the surface of ZIF-8. The Cu@ZIF-8 sample exhibits a higher contact angle of  $109.9 \pm 1.6^\circ$ , which is disadvantageous for the electro-catalytic reaction in water phase. On the other hand, the contact angle of HHN material has sharply declined to  $31.2 \pm 0.6^\circ$ , indicating that the hydrophobic ZIF-8 has turned into hydrophilic HHNs after the organic weak acid etching. The lower contact angle of HHNs may be contributed to the carboxylate groups of residual GA and the exposed polar groups on HHNs. The contact angle on Cu@HHNs is slightly increased to  $36.3^\circ \pm 0.9^\circ$ . This low value is highly desirable for aqueous electrochemical reaction. Thus, the catalyst Cu@HHNs is expected to yield favorable electrochemical performance toward glucose oxidation in view of its hydrophilic surface and the hierarchically-porous structure.

In order to optimize the electro-catalytic performance of the catalyst Cu@HHNs toward non-enzymatic glucose sensing, the parameters which can influence the synthesis of the material was studied. A series of experiments on the effects of etching time and concentration of the etching acid were carried out. As depicted in the Fig. S7, the experiments yield that the optimized time of etching is 10 min and the optimized concentration of the etching acid is  $12\text{ g/L}$ . Thus, the catalyst Cu@HHNs that was etched in  $12\text{ g/L}$  GA for 10 min is employed for the next series of experiment.

### 3.2. Electrochemical performance of Cu@HHNs based sensor

First, the loading amount of the catalyst on GCE was optimized by using CVs in  $10\text{ mM}$  glucose and  $0.1\text{ M}$  NaOH solution because it plays a crucial role in the electrochemical performance of catalyst. The peak currents of glucose in CVs during positive scans first increase, reaching a peak when the loading of Cu@HHNs is  $16\text{ }\mu\text{g}$ , and then reduce gradually, as depicted in Fig. S8. The increase of peak currents is attributed to the augment of the catalytic active sites. However, more loading amount of the catalyst decreases the peak currents owing to larger mass transfer resistance when the active sites are buried deeper in catalyst-modified layer. Therefore,  $16\text{ }\mu\text{g}$  is the optimal loading amount of the catalyst, which is adopted in the following experiment.

To characterize the electrochemical performance of catalyst, CVs were studied in the absence and presence of  $10\text{ mM}$  glucose in  $0.1\text{ M}$  NaOH, as shown in Fig. 5. In Fig. 5A, characteristic redox peaks of ZIF-8

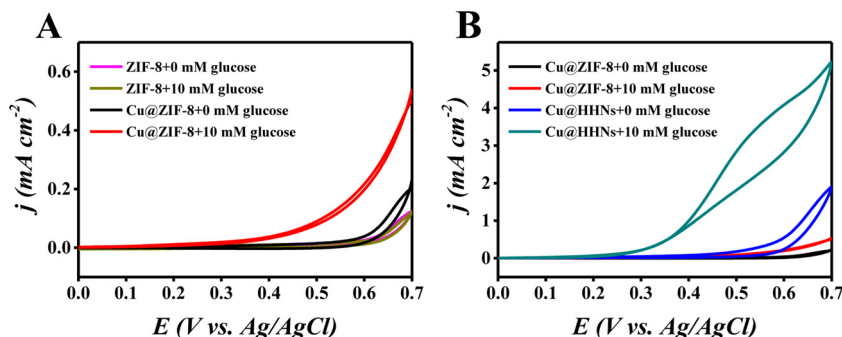
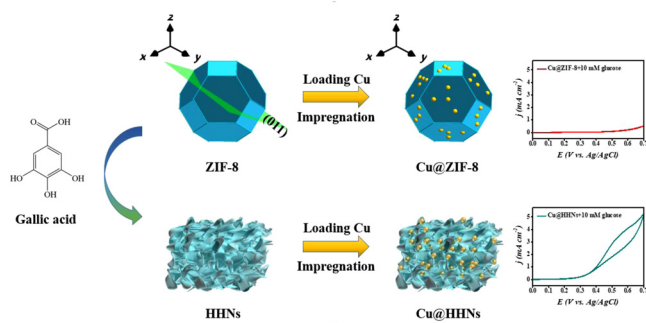


Fig. 5. Cyclic voltammograms of ZIF-8, Cu@ZIF-8, HHNs, and Cu@HHNs with the absence and presence of  $10\text{ mM}$  glucose in  $0.1\text{ M}$  NaOH. The scan rate:  $10\text{ mV s}^{-1}$ .



could not be found in the set potential window in 0.1 M NaOH owing to the fact that the redox potential of the  $\text{Zn}^{2+}/\text{Zn}^0$  pair was outside of the examined range [22]. Moreover, there is negligible change in the current density toward the electrolyte with or without glucose, indicating that the matrix ZIF-8 makes negligible contribution to the glucose electro-catalytic oxidation. After Cu is loaded on the ZIF matrix, Cu@ZIF-8 provides stronger background current signal than ZIF-8, indicating that Cu@ZIF-8 possesses better performance than ZIF-8 in electron transfer in alkaline medium (0.1 M NaOH) owing to the electrochemical activity of copper. With the increase of the electrode potential, Cu is initially oxidized to CuO and further to CuOOH in alkaline medium. The Cu(III) state is unstable and has the high ability to oxidize glucose. When in alkaline medium, glucose molecule is deprotonated and isomerized into an enediol structure, which can get an electron from CuOOH and is oxidized into gluconolactone (Equation 1). Then after hydrolysis, gluconic acid is produced [8,22]. Therefore, with the presence of 10 mM glucose in the electrolyte, the anodic current on Cu@ZIF-8 electrode undergoes a considerable rise at the onset potential of about +0.35 V, indicating the irreversible glucose electro-oxidation.



As depicted in Fig. 5B, it is obvious that Cu@HHNs presents superior ability to catalyze glucose oxidation, comparing with Cu@ZIF-8. This superior catalytic ability arises from etching the matrix ZIF-8 with organic weak acid to transform hydrophobic homogeneous-porous matrix ZIF-8 into hydrophilic hierarchy-porous nanoflowers.

Amperometric measurements were implemented at +0.6 V via successive injection of glucose into 0.1 M NaOH under continuous stirring, as illustrated in Fig. 6A. Fig. 6B displays the relationship between the current signal detected and the concentration of glucose added. It can be inferred from Fig. 6B that the Cu@HHNs based sensor displays linear current response against glucose concentration from 5  $\mu\text{M}$  to 3 mM with a sensitivity of  $1594.2 \mu\text{A cm}^{-2} \text{mM}^{-1}$  ( $R^2 = 0.995$ ). Moreover, the limit of detection (LOD) is estimated to be  $1.97 \mu\text{M}$  (corresponding to signal-to-noise ratio of 3). Table 1 provides a comparison between Cu@HHNs based sensor and various other Cu-based nanomaterials reported in literature [14,22,32–39], highlighting the high sensitivity of the Cu@HHNs based sensor reported here.

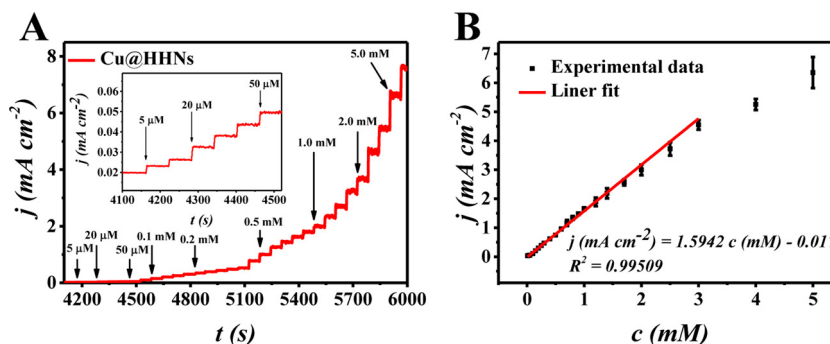


Fig. 6. (A) Chronoamperometric response of the Cu@HHNs based sensor to successive addition of glucose into 0.1 M NaOH. (B) Scatter plot of current density vs. added glucose concentration. Applied potential: +0.6 V.

Table 1

Comparison of sensing performances of the Cu@HHNs based sensor with other Cu-based nonenzymatic electrochemical glucose sensors.

Catalysts	Sensitivity ( $\mu\text{A mM}^{-1} \text{cm}^{-2}$ )	Linear range (mM)	Detection limit ( $\mu\text{M}$ )	Refs
Cu@HHNs	1594.2	0.005–3	1.97	This work
Cu in ZIF-8	418	0–0.7	2.76	[22]
MCOF-4	224	–	4.22	[39]
Cu@CoOx	396.57	0.001–5	0.1	[38]
resin-Cu <sup>2+</sup>	–	0.005–1	1.8	[35]
M/MO@C-800	–	0.0001–2.2	0.06	[37]
mesoporous Au-Cu	643.6	0.01–19	1.5	[34]
mesoporous Cu	606	0–10	0.2	[14]
Cu NPs/Graphene	430.52	0.01–1	7.2	[36]
CuO-CS	503.129	0.05–1	11	[32]
Cu-Pd	298	0.01–9.6	0.32	[33]

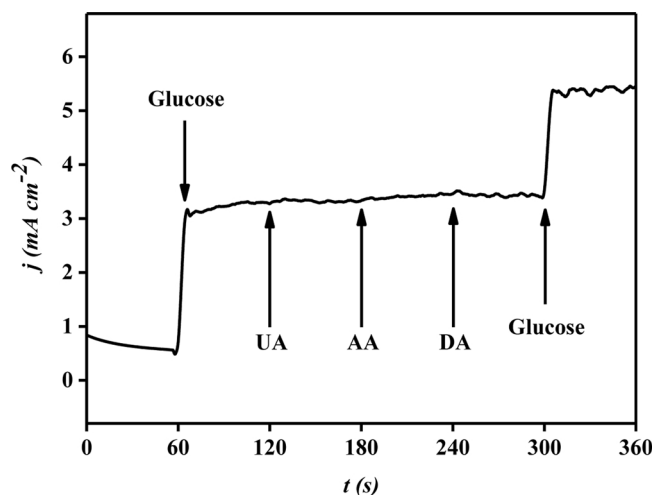


Fig. 7. Chronoamperometric response of the Cu@HHNs based sensor on sequential addition of 2 mM glucose, 0.1 mM uric acid (UA), 0.1 mM ascorbic acid (AA) and 0.1 mM dopamine (DA) into 0.1 M NaOH. Applied potential: +0.6 V.

Considering that the loading of the catalyst is approximately  $0.22 \text{ mg/cm}^2$ , which is 60% higher than that in literature [22], the sensitivity of the Cu@HHNs based sensor is 3.8 times as high as that in the literature. It further confirms the superior performance of the Cu@HHNs based sensor reported here. According to the loading amount, the sensitivity of the Cu@HHNs based sensor was also compared to those in literature, as shown in Table S3.

### 3.3. Selectivity and stability of the Cu@HHNs based sensor

The selectivity of the Cu@HHNs based sensor is also assessed by



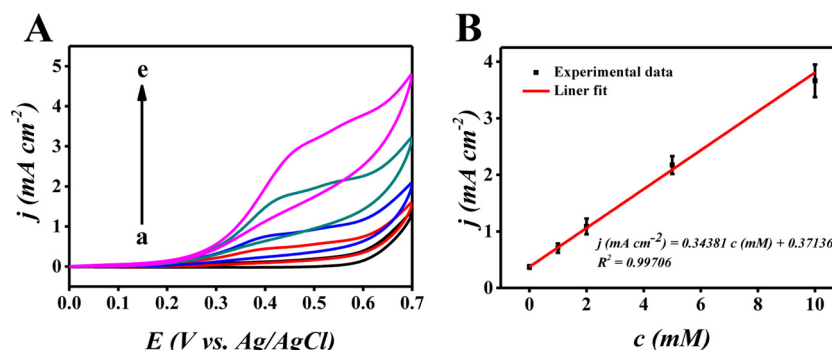


**Fig. 8.** (A) CV curves of the Cu@HHNs based sensor in human blood serum sample (10%) in 0.1 M NaOH with the presence of varied glucose concentrations: (a) 0, (b) 1, (c) 2, (d) 5, and (e) 10 mM from inner to outer. The scan rate is set as  $10 \text{ mV s}^{-1}$ . (B) The corresponding calibration curve at +0.6 V.

means of documenting the current signals via injecting 0.1 mM of interfering species uric acid (UA), ascorbic acid (AA) and dopamine (DA) into the original alkaline environment. As illustrated in Fig. 7, when UA, AA and DA are successively injected into the system, the signal does not change. Given the fact that the concentration of glucose in physiological environment is 30 times higher than the concentration of those interfering species [40,41], the selectivity of the Cu@HHNs based sensor is promising.

In order to highlight the stability of Cu@HHNs for the non-enzymatic glucose sensing, the current changes of the Cu@HHNs based sensor and the Cu@ZIF-8 based sensor during continuous monitoring of glucose were recorded, as shown in Fig. S9. After 40 circles of cyclic voltammetry test, the normalized activity of the Cu@ZIF-8 based sensor can still reach 74.5% of the initial activity, which is satisfactory. Interestingly, the normalized activity of the Cu@HHNs based sensor can even reach 91.8% of the initial activity after the same long recycling test. This prominent stability of the Cu@HHNs based sensor may be ascribed to the unique spatial structure of the reconstructed ZIF-8, which consists of hydrophilic hierarchically-porous nanoflowers. The polar centers of HHNs are exposed by acid etching, thus making the catalytic nanoparticles adsorbed firmly on the HHN matrix, thereby effectively protecting Cu NPs from migration, agglomeration, and dissolution in the course of the electro-catalytic process. As a consequence, the electro-catalytic performance of Cu NPs toward the non-enzymatic glucose sensing could be retained to a large extent after recycling use, thus ensuring the stability of the Cu@HHNs based sensor.

### 3.4. Validation of analytical principle

In order to examine its feasibility for practical sample testing, the Cu@HHNs based sensor was exploited to detect glucose in human blood serum. Fig. 8A illustrates that the current density of the oxidation peak increase gradually with the concentration of glucose added into the diluted blood serum sample (10%). The corresponding calibration curve (Fig. 8B) suggests that the current density of the oxidation peak possesses a good linear relationship with the concentration of glucose ranging from 0 to 10 mM. Considering that the concentration level of glucose in the physiological condition is between 4 and 7 mM [40], the Cu@HHNs based sensor is very promising for nonenzymatic glucose sensing in practical sample testing under alkaline conditions.

## 4. Conclusions

In conclusion, the Cu@HHNs based sensor has been demonstrated as an efficient transducer for glucose electro-catalytic oxidation under alkaline conditions. In particular, the Cu@HHNs based sensor displays exceptional sensing performances with a linear range of  $5 \mu\text{M}$  to  $3 \text{ mM}$ , a detection limit of  $1.97 \mu\text{M}$ , a sensitivity of  $1594.2 \mu\text{A mM}^{-1} \text{ cm}^{-2}$ , and high selectivity, specificity, and reproducibility. This research not only provides a promising catalyst with high performance toward non-

enzymatic glucose sensing but would offer a new approach to controllably adjust the structure of a porous material by one particular organic weak acid, change its intrinsic property and enhance its catalytic performance for analytical applications.

## CRediT authorship contribution statement

**Qizhen Zhu:** Investigation. **Shiyu Hu:** Validation. **Linqun Zhang:** Investigation. **Ying Li:** Writing - original draft, Supervision. **Carlo Carraro:** Writing - review & editing. **Roya Maboudian:** Conceptualization. **Wei Wei:** Funding acquisition. **Anran Liu:** Funding acquisition. **Yuanjian Zhang:** Resources. **Songqin Liu:** Resources.

## Declaration of Competing Interest

The authors declare that they have no known competing financial interests or personal relationships that could have appeared to influence the work reported in this paper.

## Acknowledgements

We would like to thank the National Natural Science Foundation of China (grant no. 21775019), the Industrial Members of the Berkeley Sensor & Actuator Center (BSAC) and the US National Science Foundation (grant no. 1903188) for their support of this project.

## Appendix A. Supplementary data

Supplementary material related to this article can be found, in the online version, at doi:<https://doi.org/10.1016/j.snb.2020.128031>.

## References

- [1] L.J. Mandarino, A. Consoli, A. Jain, D.E. Kelley, Differential regulation of intracellular glucose-metabolism by glucose and insulin in human muscle, *Am. J. Physiol.* 265 (1993) E898–E905.
- [2] P. Deedwania, M. Kosiborod, E. Barrett, A. Ceriello, W. Isley, T. Mazzone, P. Raskin, Hyperglycemia and acute coronary syndrome - A scientific statement from the American heart association diabetes committee of the council on nutrition, physical activity, and metabolism, *Circulation* 117 (2008) 1610–1619.
- [3] X. Cao, N. Wang, S. Jia, Y. Shao, Detection of glucose based on bimetallic PtCu nanochains modified electrodes, *Anal. Chem.* 85 (2013) 5040–5046.
- [4] A. Pandey, P. Tripathi, R. Pandey, R. Srivastava, S. Goswami, Alternative therapies useful in the management of diabetes: A systematic review, *J. Pharm. Bioallied Sci.* 3 (2011) 504–512.
- [5] G. Rocchitta, O. Secchi, M.D. Alvau, D. Farina, G. Bazzu, G. Calia, R. Migheli, M.S. Desole, R.D. O'Neill, P.A. Serra, Simultaneous telemetric monitoring of brain glucose and lactate and motion in freely moving rats, *Anal. Chem.* 85 (2013) 10282–10288.
- [6] A. Heller, B. Feldman, Electrochemical glucose sensors and their applications in diabetes management, *Chem. Rev.* 108 (2008) 2482–2505.
- [7] J. Wang, Electrochemical glucose biosensors, *Chem. Rev.* 108 (2008) 814–825.
- [8] R. Ahmad, M. Vaseem, N. Tripathy, Y.B. Hahn, Wide linear-range detecting non-enzymatic glucose biosensor based on CuO nanoparticles inkjet-printed on



- electrodes, *Anal. Chem.* 85 (2013) 10448–10454.
- [9] T. Chen, D. Liu, W. Lu, K. Wang, G. Du, A.M. Asiri, X. Sun, Three-dimensional Ni<sub>2</sub>P nanoarray: an efficient catalyst electrode for sensitive and selective nonenzymatic glucose sensing with High specificity, *Anal. Chem.* 88 (2016) 7885–7889.
  - [10] K. Dhara, D.R. Mahapatra, Electrochemical nonenzymatic sensing of glucose using advanced nanomaterials, *Microchim. Acta* 185 (2017) 49.
  - [11] H.Y. Jiang, P. Zhou, Y. Wang, R. Duan, C. Chen, W. Song, J. Zhao, Copper-based coordination polymer nanostructure for visible light photocatalysis, *Adv. Mater.* 28 (2016) 9776–9781.
  - [12] J.J. Lv, M. Jouny, W. Luc, W. Zhu, J.J. Zhu, F. Jiao, A highly porous copper electrocatalyst for carbon dioxide reduction, *Adv. Mater.* 30 (2018) e1803111.
  - [13] C. Zhang, K. Xu, W. Zhou, X. Lu, R. Li, G. Li, Copper-antimony alloy-nanoparticle clusters supported on porous Cu networks for electrochemical energy storage, *Part. Part. Syst. Charact.* 33 (2016) 553–559.
  - [14] C.L. Li, B. Jiang, Z.L. Wang, Y.Q. Li, M.S.A. Hossain, J.H. Kim, et al., First synthesis of continuous mesoporous copper films with uniformly sized pores by electrochemical soft templating, *Angew. Chem. Int. Ed.* 55 (2016) 12746–12750.
  - [15] H. Li, C.Y. Guo, C.L. Xu, A highly sensitive non-enzymatic glucose sensor based on bimetallic Cu-Ag superstructures, *Biosens. Bioelectron.* 63 (2015) 339–346.
  - [16] Z. Gao, J. Liu, J. Chang, D. Wu, J. He, K. Wang, F. Xu, K. Jiang, Mesocrystalline Cu<sub>2</sub>O hollow nanocubes: synthesis and application in non-enzymatic amperometric detection of hydrogen peroxide and glucose, *Cryst. Eng. Comm.* 14 (2012) 6639.
  - [17] K. An, S. Alayoglu, N. Musselwhite, S. Plamthottam, G. Melaet, A.E. Lindeman, G.A. Somorjai, Enhanced CO oxidation rates at the interface of mesoporous oxides and Pt nanoparticles, *J. Am. Chem. Soc.* 135 (2013) 16689–16696.
  - [18] L. Du, M. Yuan, H. Wei, X. Xing, D. Feng, Y. Liao, H. Chen, D. Yang, Interconnected Pd nanoparticles supported on zeolite-AFI for hydrogen detection under ultralow temperature, *ACS Appl. Mater. Interfaces* 11 (2019) 36847–36853.
  - [19] J. Song, F. Wang, X. Yang, B. Ning, M.G. Harp, S.H. Culp, et al., Gold nanoparticle coated carbon nanotube ring with enhanced raman scattering and photothermal conversion property for theranostic applications, *J. Am. Chem. Soc.* 138 (2016) 7005–7015.
  - [20] M. Zhuang, X. Ou, Y. Dou, L. Zhang, Q. Zhang, R. Wu, Y. Ding, M. Shao, Z. Luo, Polymer-embedded fabrication of Co<sub>2</sub>P nanoparticles encapsulated in N,P-doped graphene for hydrogen generation, *Nano Lett.* 16 (2016) 4691–4698.
  - [21] A. Phan, C.J. Doonan, F.J. Uribe-Romo, C.B. Knobler, M. O'keeffe, O.M. Yaghi, Synthesis, structure, and carbon dioxide capture properties of zeolitic imidazolate frameworks *Acc. Chem. Res.* 43 (2009) 58–67.
  - [22] L. Shi, X. Zhu, T. Liu, H. Zhao, M. Lan, Encapsulating Cu nanoparticles into metal-organic frameworks for nonenzymatic glucose sensing, *Sens. Actuators B: Chem.* 227 (2016) 583–590.
  - [23] Y. Liu, Z. Li, Q. Yu, Y. Chen, Z. Chai, G. Zhao, et al., A General strategy for fabricating isolated single metal atomic site catalysts in Y zeolite, *J. Am. Chem. Soc.* 141 (2019) 9305–9311.
  - [24] R. Yang, X. Yan, Y. Li, X. Zhang, J. Chen, Nitrogen-doped porous carbon-ZnO nanopolyhedra derived from ZIF-8: New materials for photoelectrochemical biosensors, *ACS Appl. Mater. Interfaces* 9 (2017) 42482–42491.
  - [25] X. Niu, M. Lan, H. Zhao, C. Chen, Highly sensitive and selective nonenzymatic detection of glucose using three-dimensional porous nickel nanostructures, *Anal. Chem.* 85 (2013) 3561–3569.
  - [26] X. Yang, J. Sun, M. Kitta, H. Pang, Q. Xu, Encapsulating highly catalytically active metal nanoclusters inside porous organic cages, *Nat. Catal.* 1 (2018) 214–220.
  - [27] T. Zhuang, Y. Pang, Z. Liang, Z. Wang, Y. Li, C. Tan, et al., Copper nanocavities confine intermediates for efficient electrosynthesis of C<sub>3</sub> alcohol fuels from carbon monoxide, *Nat. Catal.* 1 (2018) 946–951.
  - [28] D. Gao, R. Liu, J. Biskupek, U. Kaiser, Y.F. Song, C. Streb, Modular design of noble-metal-free mixed metal oxide electrocatalysts for complete water splitting, *Angew. Chem. Int. Ed.* 58 (2019) 4644–4648.
  - [29] P. Liu, E.J. Hensen, Highly efficient and robust Au/MgCuCr<sub>2</sub>O<sub>4</sub> catalyst for gas-phase oxidation of ethanol to acetaldehyde, *J. Am. Chem. Soc.* 135 (2013) 14032–14035.
  - [30] G. Liang, A. Wang, L. Li, G. Xu, N. Yan, T. Zhang, Production of primary amines by reductive amination of biomass-derived Aldehydes/Ketones, *Angew. Chem. Int. Ed.* 56 (2017) 3050–3054.
  - [31] X. Zhao, P. Pachfule, S. Li, T. Langenhahn, M. Ye, C. Schlesiger, S. Praetz, J. Schmidt, A. Thomas, Macro/Microporous covalent organic frameworks for efficient electrocatalysis, *J. Am. Chem. Soc.* 141 (2019) 6623–6630.
  - [32] M. Figiela, M. Wysokowski, M. Galinski, T. Jesionowski, I. Stepniak, Synthesis and characterization of novel copper oxide-chitosan nanocomposites for non-enzymatic glucose sensing, *Sens. Actuators B: Chem.* 272 (2018) 296–307.
  - [33] Z. Li, X. Zhao, X. Jiang, Y. Wu, C. Chen, Z. Zhu, J. Marty, Q. Chen, An enhanced nonenzymatic electrochemical glucose sensor based on copper-palladium nanoparticles modified glassy carbon electrodes, *Electroanalysis* 30 (2018) 1811–1819.
  - [34] A.S. Nugraha, V. Malgras, M. Iqbal, B. Jiang, C. Li, Y. Bando, A. Alshehri, J. Kim, Y. Yamauchi, T. Asahi, Electrochemical synthesis of mesoporous Au-Cu alloy films with vertically oriented mesochannels using block copolymer micelles, *ACS Appl. Mater. Interfaces* 10 (2018) 23783–23791.
  - [35] M.A.P. Papi, M.F. Bergamini, L.H. Marcolino-Junior, Electrochemical behavior of a cation-exchange resin modified with copper ions on non-enzymatic glucose determination, *J. Electroanal. Chem.* 835 (2019) 248–253.
  - [36] T. Soganci, R. Ayrançi, E. Harputlu, K. Okakoglu, M. Acet, M. Farle, C.G. Unlu, M. Ak, An effective non-enzymatic biosensor platform based on copper nanoparticles decorated by sputtering on CVD graphene, *Sens. Actuators B: Chem.* 273 (2018) 1501–1507.
  - [37] X. Xiao, S. Peng, C. Wang, D. Cheng, N. Li, Y. Dong, et al., Metal/metal oxide@carbon composites derived from bimetallic Cu/Ni-based MOF and their electrocatalytic performance for glucose sensing, *J. Electroanal. Chem.* 841 (2019) 94–100.
  - [38] R. Yuan, H. Li, X. Yin, P. Wang, J. Lu, L. Zhang, Cu nanowires paper interlinked with cobalt oxide films for enhanced sensing and energy storage, *Chem. Commun.* 55 (2019) 9031–9034.
  - [39] J. Zhang, X. Wang, J. Lv, D.S. Li, T. Wu, A multivalent mixed-metal strategy for single-Cu(+) ion-bridged cluster-based chalcogenide open frameworks for sensitive nonenzymatic detection of glucose, *Chem. Commun.* 55 (2019) 6357–6360.
  - [40] C. Guo, H. Huo, X. Han, C. Xu, H. Li, Ni/CdS bifunctional Ti@TiO<sub>2</sub> core-shell nanowire electrode for high-performance nonenzymatic glucose sensing, *Anal. Chem.* 86 (2014) 876–883.
  - [41] Y. Su, B. Luo, J.Z. Zhang, Controllable cobalt oxide/Au hierarchically nanostructured electrode for nonenzymatic glucose sensing, *Anal. Chem.* 88 (2016) 1617–1624.
- Qizhen Zhu** Graduate student at School of Chemistry and Chemical Engineering, Southeast University, Nanjing 211189, China.
- Shiyu Hu** Undergraduate student at School of Chemistry and Chemical Engineering, Southeast University, Nanjing 211189, China.
- Linqun Zhang** Ph.D. School of Chemistry and Chemical Engineering, Southeast University. Associate Professor at Analytical & Testing Center, Nanjing Normal University, Nanjing 210023, China.
- Ying Li** Ph.D. Nanjing University. Visiting Scholar at Department of Chemical and Biomolecular Engineering, University of California, Berkeley, California 94720, USA. Associate Professor at School of Chemistry and Chemical Engineering, Southeast University, Nanjing 211189, China.
- Carlo Carraro** Adjunct Professor at Department of Chemical and Biomolecular Engineering, University of California, Berkeley, California 94720, USA
- Roya Maboudian** Ph.D. California Institute of Technology. Postdoctor at IBM
- Wei Wei** Ph.D. Nanjing University. Professor at School of Chemistry and Chemical Engineering, Southeast University, Nanjing 211189, China.
- Anran Liu** Ph.D. Qinghua University. Associate Professor at School of Chemistry and Chemical Engineering, Southeast University, Nanjing 211189, China.
- Yuanjian Zhang** Ph.D. Changchun Institute of Applied Chemistry, Chinese Academy of Sciences, China Professor Southeast University, China. Researcher International Center for Young Scientists, National Institute for Materials Science, Japan. Postdoctor Max Planck Institute of Colloids and Interfaces, Germany
- Songqin Liu** Ph.D. Nanjing University. Professor at School of Chemistry and Chemical Engineering, Southeast University, Nanjing 211189, China.